J. Micromech. Microeng. **19** (2009) 105012 (8pp) doi:10.1088/0960-1317/19/10/105012

Thermo-rheological behaviour of polymer melts in microinjection moulding

J C Vasco[1], J M Maia[2,3] and A S Pouzada[2]

[1] Department of Mechanical Engineering, Polytechnic Institute of Leiria, Leiria, Portugal
[2] Institute for Polymers and Composites, University of Minho, Guimarães, Portugal
[3] Department of Macromolecular Science and Engineering, Case Western Reserve University, Cleveland, OH, USA

E-mail: asp@dep.uminho.pt

Received 7 May 2009, in final form 3 August 2009
Published 17 September 2009
Online at stacks.iop.org/JMM/19/105012

Abstract
Microinjection has proven to be one of the most efficient replication methods for microcomponents and microsystems in various domains of microengineering. The use of available commercial microinjection equipment to evaluate the polymeric flow in microchannels would surely contribute to enhancing knowledge on polymeric flow at the microscale under industrial conditions. This approach is appropriate since rheological phenomena such as wall slip, surface tension, melt pressure drop and polymer flow length can be studied. These aspects are not fully dealt with in current commercial simulation software packages. In this study a micromould was designed to assess and characterize the flow in microchannels under realistic industrial conditions.

1. Introduction

Microinjection moulding is one of the most flexible, reliable and effective replication methods for microcomponents and microsystems for high-demand client industries such as medical applications, personal well-being, automobile and aerospace industry, and military and defence applications (Martin *et al* 2003). Along with microhot embossing, this process has played a major role in bringing to the market several microsystems at reasonable end-user prices such as microelectro/mechanical components, microoptic systems and microfluidic devices (Giboz *et al* 2007, Zhao *et al* 2003). The massification of microtechnologies depends directly on the effectiveness of their production (Piotter *et al* 1997). The market for microcomponents obtained by microinjection is growing, showing high business potential and is surely becoming one of the key technologies for micromanufacturing (Sha *et al* 2005). The need for quickly and accurately getting the moulding zone of moulds for microinjection moulding originated the development of the Variotherm system (Piotter *et al* 2002). The original system was the object of various developments as recently reviewed by Giboz and co-workers(Giboz *et al* 2007). These systems are for the accurate replication of high-aspect-ratio microstructures, and precise process control as is the case of optical components (Piotter *et al* 2002, Giboz *et al* 2007). Despite its success in the replication of microdetails, as in CDs or DVDs, the polymer filling behaviour of mould cavities still requires further study since the simulation tools currently available cannot fully predict flow effects at the microscale. Aspects such as wall slip, surface tension and heat transfer phenomena, require further study to avoid or minimize re-engineering costs or even to prevent wrong options in the microcomponent or microsystem design (Kim *et al* 2002, Piotter *et al* 2002, Su *et al* 2004).

2. Flow models

The viscosity of liquids and polymer solutions flowing in microchannels has been observed to increase up to 80% near the wall of the channel. During the polymer flow such an effect is believed to be due to its high intermolecular interaction and the disentanglements between bulk and wall chains (Eringen and Okada 1995, Awati *et al* 2000). Effects such as microscale viscosity, wall slip and surface tension need to be studied for a full comprehension of the rheological behaviour of the flow in microchannels (Yao and Kim 2002).

2.1. Capillary and slit flow models

The polymer flow in microchannels is quite similar to that in capillary viscosity measurements (Chien *et al* 2005, Hatzikiriakos and Dealy 1992, Rosenbaum and Hatzikiriakos 1997, Sha *et al* 2005). These measurements are based on the relationships between the pressure drop along the capillary channel and the imposed flow rate (Carreau *et al* 1997). For capillary rheometry, the following assumptions are made:

- the Reynolds number (*Re*) is smaller than 2000; thus, laminar flow is occurring;
- steady state, $\frac{\partial}{\partial t} = 0$;
- there is a fully developed unidirectional flow: $V_r = V_\theta = 0$ and $V_z = V_z(r)$ and
- there is no slip at the capillary walls: $V_z(r = R) = 0$ and $\frac{dV_z}{dr} = \frac{dV_z}{dr}(\sigma_{rz})$.

Considering the microchannel geometry to be used, the mathematical models used to describe the polymer flow are the same as for capillary rheometry (equation (1)) and slit flow:

$$\dot{\gamma}_{w(app)} = \frac{4Q}{\pi \cdot R^3}. \tag{1}$$

After the Rabinowitsch procedure for the shear rate at the wall, the following equation for the non-Newtonian fluid shear rate results in equation (2) (Chen *et al* 2008):

$$\dot{\gamma}_{w(real)} = \frac{4Q}{\pi \cdot R^3}\left(\frac{3}{4} + \frac{1}{4}n\right), \tag{2}$$

where Q is the volumetric flow rate, R is the radius of the capillary channel and n is the slope obtained by the bi-logarithmic correlation between $\log \dot{\gamma}_{w(app)}$ and $\log \tau_w$.

Furthermore, the Bagley correction is applied to the apparent shear stress τ_w, given by equation (3), in order to eliminate the viscous and elastic effects on the capillary entrance:

$$\tau_{w(app)} = \frac{\Delta P}{2L}R. \tag{3}$$

The shear stress at the wall is now given by equation (4) (Chen *et al* 2008):

$$\tau_{w(real)} = \frac{\Delta P}{2\left(\frac{L}{R} + e\right)} = \frac{\Delta P - P_0}{2L}R, \tag{4}$$

where ΔP is the pressure drop along the capillary, L and R are the length and radius of the capillary, e is the Bagley correction factor and P_0 is the pressure drop for a capillary with zero length for a given rate of shear.

The slit flow model also derives from the equations used for the capillary viscometer in a similar way to the previous flow models. A microchannel must be designed to meet the requirements of a slit flow, enabling pressure monitoring at both ends to generate specific experimental data (figure 1).

The apparent shear rate of a slit is given by

$$\dot{\gamma}_{w(app)} = \frac{6Q}{w \cdot h^2}. \tag{5}$$

After applying the Walter correction for non-Newtonian fluids (Chen *et al* 2008), it becomes

$$\dot{\gamma}_{w(real)} = \frac{6Q}{w \cdot h^2}\left(\frac{2}{3} + \frac{1}{3}n\right), \tag{6}$$

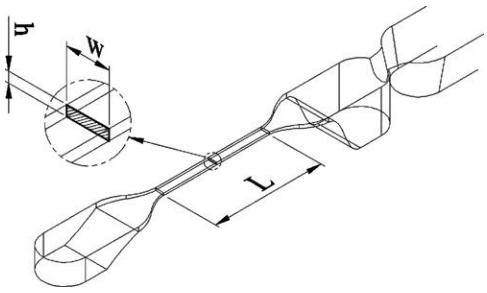

Figure 1. Overall dimensions of a slit channel.

where Q is the volumetric flow rate, w and h are width and height of the rectangular cross-sectioned channel, respectively, and n is the slope obtained by the bi-logarithmic correlation between $\log \dot{\gamma}_{w(app)}$ and $\log \tau_w$.

In the particular case of the slit, the edge effect on the shear stress must be corrected when the width by thickness ratio is below 10. The real shear stress equation for Newtonian fluids (equation (7)) then becomes equation (8) (Chen *et al* 2008):

$$\tau_{w(real)} = \frac{h}{2}\left(\frac{-\Delta P_{real}}{L}\right) \tag{7}$$

$$\tau_{w(real)} = \frac{w \cdot h}{2(w + h)}\left(\frac{-\Delta P_{real}}{L}\right). \tag{8}$$

After the corrections on the capillary and the slit flow models, the real viscosity can be calculated for each type of flow by dividing the real shear stress by the real shear rate, resulting in equation (9) (Carreau *et al* 1997, Chen *et al* 2008):

$$\eta_{(real)} = \frac{\tau_{real}}{\dot{\gamma}_{real}}. \tag{9}$$

2.2. Wall slip effect

The concept of wall slip was first addressed by Mooney (1931), who found that certain flow curves depended on the radius of the capillary once the shear stress exceeded a critical value (Lee and Mackley 2000). The effect takes place when the shear stress at the microchannel wall exceeds a critical value, typically, above 0.1 MPa (Hatzikiriakos and Dealy 1992, Yao and Kim 2002, Mitsoulis *et al* 2005). As the magnitude of the shear stresses varies, polymer melts flow in a way that is a superposition of slipping at the wall and shearing within the melt (Gleißle and Windhab 1985). When wall slip occurs at a critical wall shear stress value the flow curves (wall shear stress versus apparent shear rate) diverge from each other and become dependant on channel dimensions. Usually the boundary conditions at the wall are known and their influence on the flow behaviour close to the wall is relevant. Assuming a constant heat flux at the wall ($\delta T/\delta r =$ constant and $Bi(T_0 - T_w)$), a simplified power-law slip model (equation (10)) was introduced for the slip velocity without considering any pressure or temperature dependence (Rosenbaum and Hatzikiriakos 1997):

$$u_s = \frac{a}{1 + (\tau_c/\tau_w)^{10}}\tau_w^m, \tag{10}$$

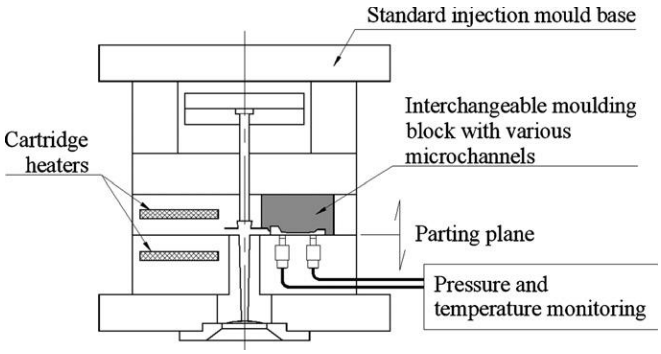

Figure 2. Concept of a tool for rheometric studies in microchannels.

where τ_w is the wall shear stress, τ_c is the critical shear stress for slip, a –is the scalar coefficient and m is the mass flow rate constancy equation given by

$$m = 2\pi \int_0^R \rho \cdot v_z \cdot r \, \mathrm{d}r. \tag{11}$$

3. Experimental methods

3.1. Concept

Currently available capillary rheometers are difficult to operate with channels with dimensions at the microregion. Alternative experimental setups guaranteeing the flow through the microchannel must generate pressure high enough and support the high stresses developed during the flow (Chien *et al* 2005). A concept meeting these requirements consists of using a small injection mould structure (100 × 130 mm) with a set of interchangeable moulding blocks with calibrated microchannels, in an injection moulding machine. The operation of such a device requires accurate temperature control during the heating and cooling phases of the moulding cycle, as well as pressure control at the extremities of the microchannel. The concept is sketched in figure 2.

It must be stressed that equipment based on this concept is not exactly a microrheometer, but it is a setup capable of replicating the flow conditions in real micromoulding situations. More precisely it is a viscometer that can be used on standard injection moulding equipment to analyse the flow using processing parameters characteristic of microinjection moulding.

The use of miniature pressure sensors and a suitable data acquisition system makes it possible to gather the information required for rheological characterization of the flow in the microchannel as suggested in figure 3.

The pressure drop, Δp, measured from the pressure sensor data is required for calculating the shear stress using equation (8). The average melt flow rate is obtained from the data acquisition system that enables the flow time between the locations of the pressure sensors, Δt, to be determined. The shear rate can then be calculated using equation (6).

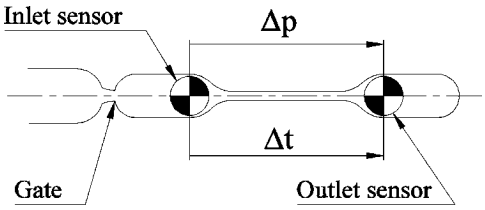

Figure 3. Variables for the rheological assessment of the flow in microchannels. Δp—pressure drop; Δt—time interval.

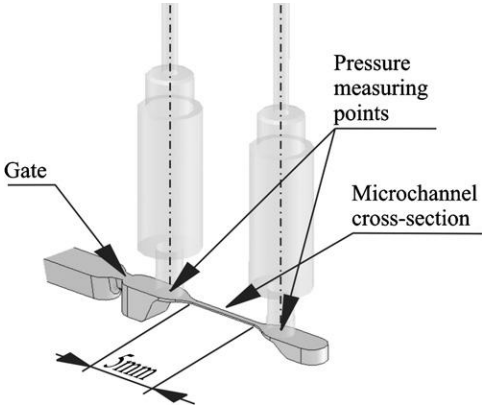

Figure 4. Layout of the microchannel and pressure sensors.

3.2. Methodology

The use of commercial microinjection moulding equipment led to the full design and development of a research mould that could be used in injection tests with various microchannels. The mould was designed to support two interchangeable moulding blocks, allowing the replacement of the microcavities. Furthermore, the tool can be used to test new types of moulding blocks, e.g. manufactured using additive technologies. Two moulding blocks with two different microchannel cross-sections were tested: a slit with a rectangular section, 400 μm wide by 100 μm deep, and a square section of 200 × 200 μm dimensions. The length of both microchannels is identical, 5 mm. The general layout of the cavities is shown in figure 4.

Concerning the location of the pressure sensors, there is a source of error that must be addressed. The physical dimensions of the commercial sensors used are from a different scale to that of the microchannel dimensions. So, the microchannels are wider at both ends to allow the assembly of the sensors for a proper pressure reading. However, such section variation causes pressure distortion and therefore an entry correction procedure for pressure drop was performed using zero-length microchannels for each cross-section tested. Therefore, two additional moulding blocks with a zero-length microchannel were manufactured to correct the measurements for entry effects (figure 5).

When the moulding blocks with microchannels are implemented, the mould can be used as a high-pressure viscometer enabling high injection pressures in the microchannels, which are difficult to achieve in conventional viscometers (Chen *et al* 2008, Chien *et al* 2005, Song *et al*

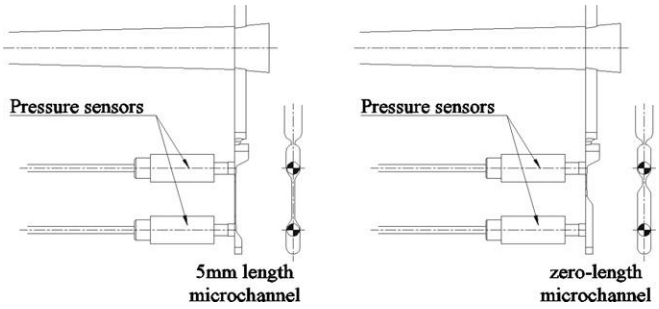

Figure 5. 2D views of the 400 × 100 μm microchannel showing the 5 mm length (on the left) and the zero-length versions (on the right).

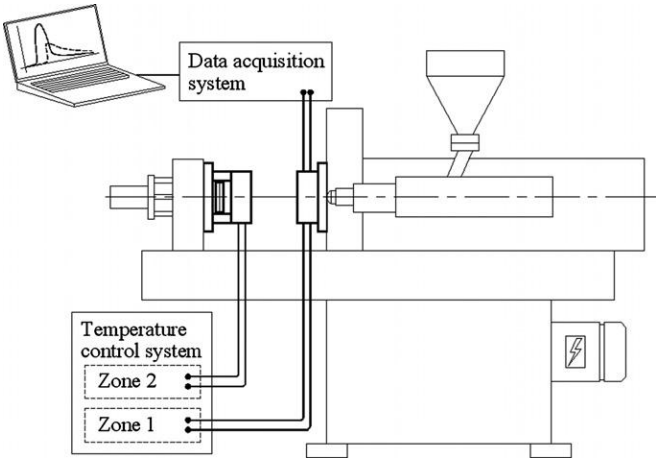

Figure 6. Layout of the injection micromoulding cell, showing the two temperature control zones and the pressure data acquisition system with sensors located on the fixed platen of the mould.

2007, Yao and Kim 2002). Since the goal is to promote the flow in microchannels, an external control unit for the heating system will provide the temperatures suitable for polymer injection at this scale, enabling quantitative flow evaluation at the same time and under the same processing conditions.

3.3. Microinjection equipment

Since the 1980s microinjection equipment has evolved to meet the requirements for microparts such as minimal shot weight and precise control of the processing conditions (pressure, injection speed, melt and mould temperatures) to achieve the high repeatability required in the applications (Piotter *et al* 2002). In this work, a Boy 12 A injection moulding machine (Dr Boy, Neustadt-Fernthal, Germany) that combines technical characteristics for microinjection and affordability (Piotter *et al* 1997, Song *et al* 2007) was used.

The microinjection cell consists of the Boy 12 A injection moulding machine with ∅14 mm injection screw, a mould temperature regulator and an external control unit for the cartridge heaters used in the temperature control system of the mould (figure 6). Concerning the injection unit ability for microinjection, the Boy 12 A machine is able to meter with high precision an injection volume as small as 0.1 cm^3 at a high flow rate, up to 15.6 cm^3 s^{-1}. The maximum injection pressure is 240 MPa.

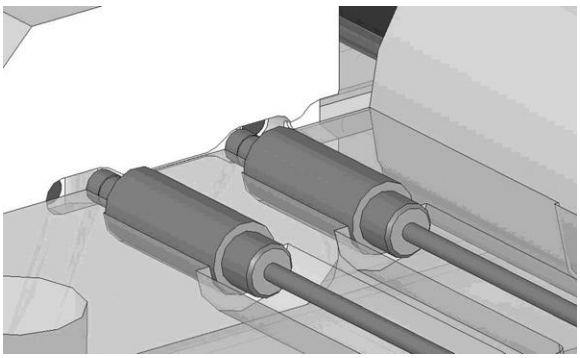

Figure 7. Assembly of the pressure sensors at the microchannel inlet and outlet.

3.4. Instrumentation

The rheological characterization of the polymer flow in the microchannel is achieved by monitoring melt pressure at the microchannel inlet and outlet using two miniature piezoelectric pressure sensors Priamus 6006B (Priamus System Technologies, Schaffenhausen, Switzerland) (figure 7). The pressure drop between the two locations and the flow velocity are used to relate the shear viscosity to the shear rate (Chen *et al* 2008, Chien *et al* 2005). The assembly of the pressure sensors is depicted in figure 7.

The data acquisition system consisted of two physical units, the input module, Multi DAQ 8101 A, and the amplifier module, Mobile DAQ 8001B, both from Priamus. The user interface was based on the Priamus Moulding Monitor software.

3.5. Materials

The injection tests were carried out with polyoxymethylene (POM), Hostaform C27021 grade from Ticona (Kelsterbach, Germany). This semi-crystalline polymer is a very easy flow injection moulding type with a MFR of 24 $cm^3/10$ min (190 °C, 2.16 kg) that is commonly used in microinjection moulding (Heckele and Schomburg 2004).

3.6. Microinjection moulding

The initial approach for the injection tests was close to conventional rheometry. The melt speed was increased gradually to establish the data required for shear rate and viscosity calculation.

Several injection speeds were imposed to reach different values of shear rate on each microchannel. For each injection speed a time interval, Δt, defined as the time lag between the melt touching each pressure transducer, was measured, enabling the calculation of the average melt speed within the microchannel. Pressure data from the inlet and outlet sensors, for typical injection moulding conditions (T_{inj} = 205 °C; T_{mould}: 145 °C; t_{inj} = 0.35 s), are shown in figure 8.

Differently from the microinjection process, no packing pressure was used since the goal was only to obtain a fully established flow within the microchannel without pressure

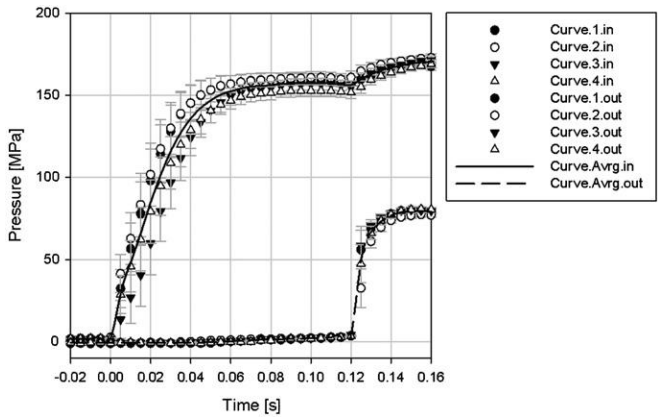

Figure 8. Typical pressure profiles during the flow in the microchannel. Suffix *in* corresponds to the signal at the channel inlet and suffix *out* at the channel outlet. The lines correspond to the average of the experimental points.

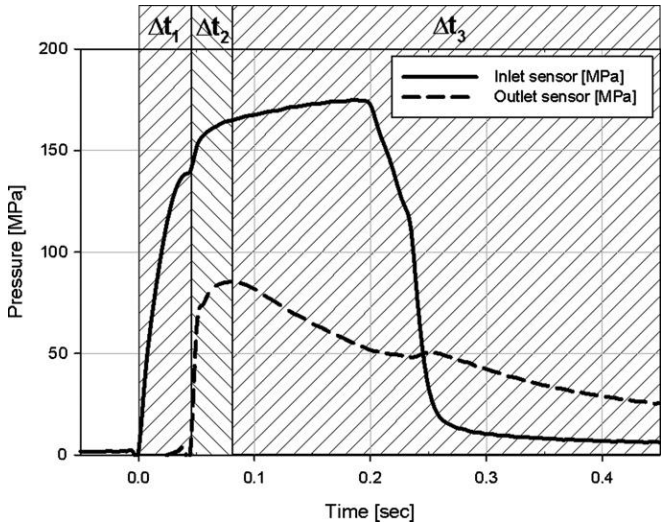

Figure 9. Sample pressure curves for the 200 × 200 μm microchannel moulding.

disturbances. The other process parameters, namely the mould and the melt temperature had to be raised gradually until complete mouldings were obtained. The 14 mm screw injection speed was varied within the capability of the equipment from 20 to 200 mm s^{-1}. The required mould temperature was 145 °C and the melt temperature was set at 235 °C. For each microchannel the data for analysis were those corresponding to full-shot mouldings, when pressure data were obtained by both pressure sensors. A typical set of data is shown in figure 9.

Three different time frames, identified as Δt_1, Δt_2 and Δt_3, can be identified in this sample. The first time frame, Δt_1, starts when the melt reaches the inlet pressure sensor at the entrance of the microchannel (solid line on the graph). The end of this interval corresponds to the instant when the melt reaches the outlet sensor at the exit of the microchannel (dashed line on the graph). After Δt_1 the flow fully develops in the microchannel, as pressure signals are recorded on both sensors, and the measurements for the viscosity evaluation can be initiated. During the second time frame, Δt_2, which ends when the outlet sensor reaches its peak, the melt fills completely the impression. After this point, the melt flow stops and the microchannel freezes off, leading to the pressure drop monitored by the two sensors. This phase occurs during the last time frame, Δt_3, where the peak on the inlet pressure sensor value corresponds to the solidification of the gate. After this point, pressure rapidly decreases as a result of the variation of the specific volume of the melt.

4. Results and discussion

4.1. Conventional rheometry

Preliminary characterization of the polymer was made using a twin-bore Rosand RH10 capillary rheometer from Malvern Instruments (Malvern, UK). The determination of traditional flow curves was carried out at the temperatures of 180 °C, 200 °C, 220 °C and 240 °C. The flow activation energy was calculated since at these temperatures, POM is a thermo-rheologically simple material and the time–temperature superposition (TTS) principle is expected to apply. For semicrystalline polymer melts and for amorphous polymer melts as well this applies when the flow temperatures are more than 100 °C above the glass transition temperature. The shift factor for each temperature, a_T, can be expressed by an Arrhenius relation (Wagner *et al* 1996) as

$$a_T = \exp\left(\frac{E}{R}\cdot\left(\frac{1}{T}-\frac{1}{T_0}\right)\right), \tag{12}$$

where E is the flow activation energy, R is the gas constant and T and T_0 are absolute temperatures.

As the TTS principle holds for this melt, the flow activation energy, E, is approximately 44 800 J K^{-1} mol. The flow curves obtained from capillary rheometry are shown in figure 10(*a*) and the master curve is depicted in figure 10(*b*).

4.2. Microchannel flow

In the injection moulding tests the mould temperature was kept at 145 °C to enable the complete filling of the impressions. This was particularly critical with the thinnest 400 × 100 μm slit microchannels. The data were obtained from fully filled mouldings, i.e. short shots were discarded.

During the tests, the two pressure profiles were recorded, from the sensors at the inlet and the outlet of the microchannel. This information, as exemplified in figure 9, allows obtaining the following information: (a) the pressure drop between inlet sensor and microchannel inlet, Δp_1; (b) the pressure drop in the microchannel itself, Δp_2 and (c) the pressure drop between the microchannel outlet and the outlet sensor, Δp_3. To determine Δp_2, the value for Δp_1 must be removed from the total pressure drop value obtained assuming that Δp_3 is much smaller than $\Sigma\Delta p_i$. The zero-length microchannel (L0) is meant to determine its initial pressure drop, which will be equivalent to Δp_1 so the values for the 5 mm microchannel (L5) could be corrected (figure 11).

In the injection tests, the melt flow rate was varied. For each condition, the time difference, Δt, was calculated between the signals of the inlet and outlet pressure sensors that

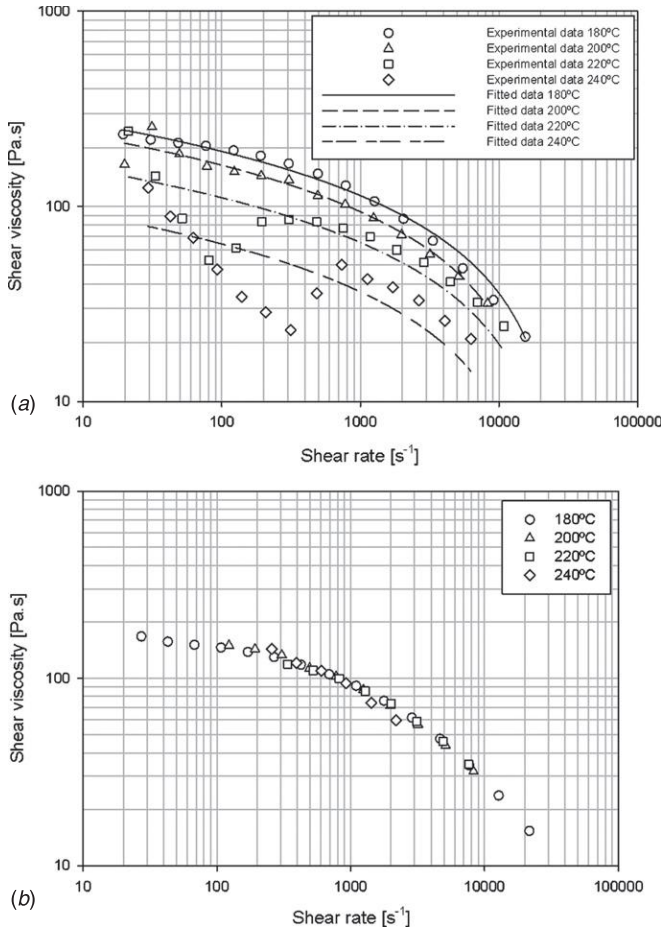

Figure 10. (*a*) Flow curves from conventional capillary rheometry for Hostaform C 27021. (*b*) Master curve for the same data, observing the time–temperature superposition principle.

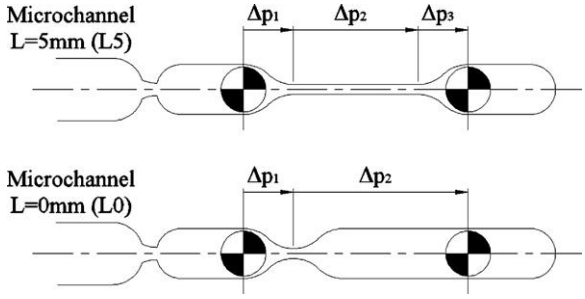

Figure 11. Determination of the pressure drop within the microchannel.

provided the flow rate value required for shear rate calculation from equation (6). The pressure drop was also obtained, allowing the calculation of shear stress through equation (8). With these two values for each melt speed, shear viscosity could be determined by the ratio between shear stress and shear rate (equation (9)) and is plotted in figure 12.

4.3. Plug flow transition

From the plot in figure 12, it is noticeable that there is an important change in the flow behaviour of each microchannel as the shear rate increases. Both curves show a transition from

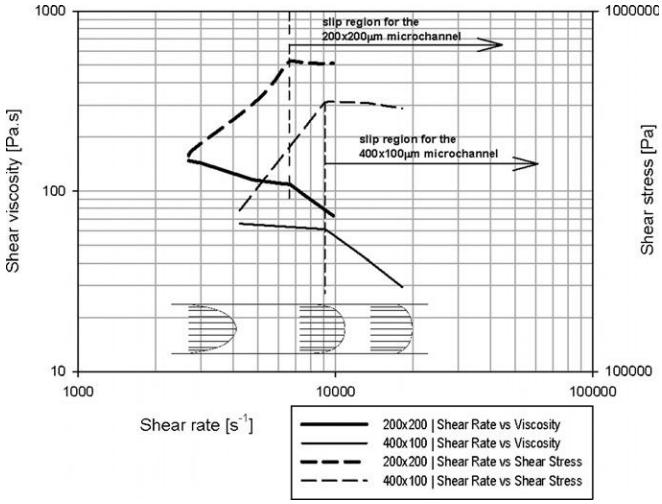

Figure 12. Flow curves from rheometry calculations based on the 200 × 200 μm and 400 × 100 μm microchannel pressure data.

a normal flow to a new type of flow where the index of non-Newtonian behaviour, n, is close to 1, indicating the onset of wall slip. The horizontal segment of both curves at constant shear stress clearly states that a change in behaviour from shear to plug flow due to the wall slip effect has occurred. The non-horizontal component of the curves corresponds to shear flow, immediately before the critical shear rate is achieved for both microchannels. It is also possible to observe in this figure that the critical shear rate for this particular material and the 200 × 200 μm microchannel is around 5000 s^{-1}. The critical shear rate for the 400 × 100 μm microchannel, for which successful shots were difficult to obtain at lower melt speeds, is estimated to be approximately 6000 s^{-1}. The different shear rate values at which the plug flow transition occurred for both microchannels can be explained by their hydraulic diameter and the aspect ratio of both cross-sections. The 200 × 200 μm square section, with an aspect ratio of 1:1, corresponds to an equivalent round section 200 μm in diameter. On the other hand, the 400 × 100 μm section with an aspect ratio of 4:1 has a hydraulic diameter of just 160 μm and therefore, a less favourable geometry for flow. This difference on the hydraulic diameter leads to a 20% decrease on the effective flow cross-section on the 400 × 100 μm microchannel, causing it to reach its critical shear rate at lower values. After these critical values of shear rate, a plug flow is fully developed in both microchannels.

4.4. Interpreting plug flow transition

Despite the processing temperature used for flow in the microchannels being 235 °C, the corresponding flow curve is located above the 180 °C flow curve, as shown in figure 13. This means that the real temperature on the microchannel is much lower than the imposed processing temperature.

Such fact is certainly due to the high surface area to volume ratio, which makes conventional heat transfer equations insufficient to describe what happens at this scale. Analysing the flow curve for the 200 × 200 μm microchannel, two segments can be observed. From A to B, shear flow

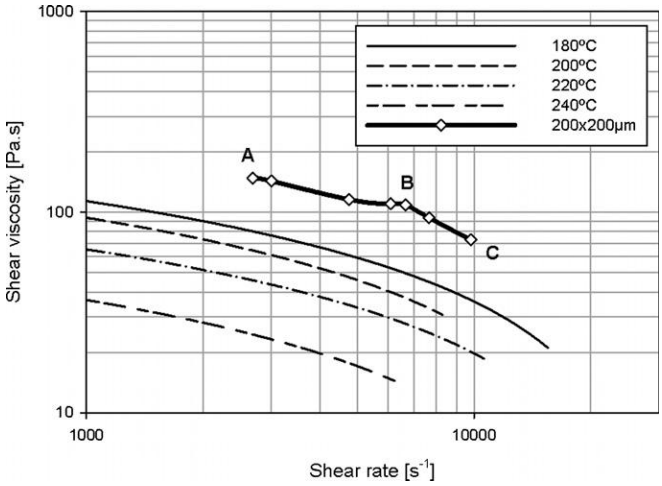

Figure 13. Plot data from conventional capillary rheometry and rheometry calculations based on the 200 × 200 μm microchannel pressure data.

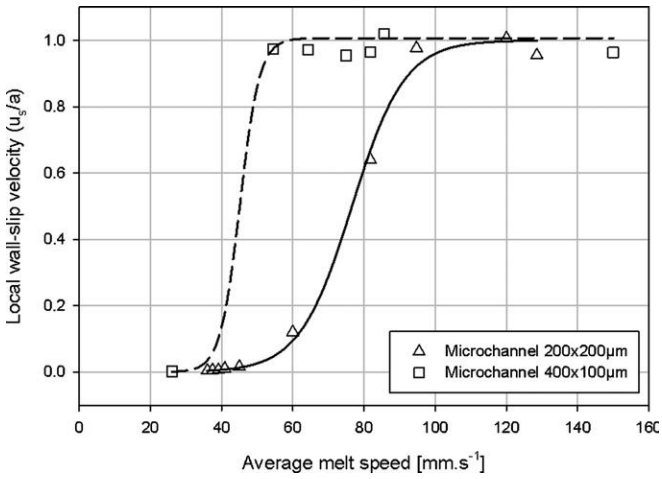

Figure 14. Plot of the average melt speed versus local wall-slip velocity.

is found although the end of this segment represents the transition to the next segment, B to C, in which plug flow is fully developed. The cooling of the molten material in the microchannel means that the temperature of the flowing melt is expected to be well below the initial 235 °C. The amplitude of the decrease, however, cannot be predicted from TTS, which is known to be valid for this material (see above). In fact, an application of TTS to the microchannel flow data in order to superimpose it with the other data yields an apparent flow temperature of less than 80 °C, which is impossible because not only it is more than 60 °C lower than the mould wall temperature, but is also lower than the no-flow temperature of POM.

This fact clearly indicates that the heat transfer analysis that is normally done in injection moulding is not directly transferable to the microscale due to the high surface area to volume ratio. Given their sub-millimetric dimensions, the microchannels exhibit a high heat diffusion rate which causes filling to occur almost isothermally (Yao and Kim 2002). In this particular case, there is effectively little or no bulk in the moulding, so our results indicate that heat transfer equations that are typically valid at the macroscale should be disregarded here.

The evaluation of the local wall slip velocity was made using equation (10). The mass flow-rate consistency value was calculated through equation (11), using the hydraulic radius of both microchannels. The melt front profile was estimated as a gradual shifting from shear flow to plug flow as shear stress increases. The data obtained for the 400 × 100 μm microchannel might not be conclusive since there are not enough data under shear flow conditions to establish a reliable trend to this value. However, the few calculated local wall slip velocity values for this microchannel seem to corroborate the conclusions already obtained on the shear stress versus shear rate plot (figure 14).

Nevertheless, both curves in figure 14 show the same trend: when shear stress is less than the critical shear stress, the local wall slip velocity is nearly zero. As predicted, the local wall slip velocity becomes close to 1 if shear stress keeps increasing (Rosenbaum and Hatzikiriakos 1997).

An immediate conclusion of this study is that the flow inside the mould is non-isothermal, which means that the data eventually obtained are not to be regarded as quantitatively accurate rheometrical data. As already stated before, the equipment setup in this study is not a microrheometer, but rather a viscometer that replicates the flow conditions in real flow situations, i.e. it is a process analyser and simulator.

5. Conclusions

In this work a tool for the quantitative evaluation of the rheological behaviour of polymer melts under typical microinjection moulding conditions was developed. The use of a microinjection moulding tool for rheometry purposes provided the establishment of flow curves for POM at pressures higher than the ones obtained on traditional rheometry, enabling critical shear rate determination for each microchannel used.

Unlike conventional capillary rheometry devices, this setup used microinjection process parameters, namely the injection speed to obtain different shear rates, enabling the plotting of flow curves. Therefore, the results could be easily applied onto the microinjection process itself or on microinjection simulation.

An important microscale effect such as wall slip was detected and the critical values of shear rate were determined for both microchannels studied. Furthermore, the local wall slip velocity was calculated and compared to the average melt velocity imposed on the process, to determine its relevance to the flow behaviour. It was noticed that the shifting between the shear flow and plug flow is much more abrupt on the 400 × 100 μm microchannel, due to the less favourable cross-section.

The results proved the validity of the experimental concept and also suggested that the heat transfer phenomena in very thin microinjection mouldings, with a very large surface area/volume ratio, play an important role that will require further study.

Acknowledgment

This research work was supported by the Portuguese Foundation for the Science and Technology under the grant SFRH/BD/36982/2007.

References

Awati K M, Park Y, Weisser E and Mackay M E 2000 Wall slip and shear stresses of polymer melts at high shear rates without pressure and viscous heating effects *J. Non-Newton. Fluid Mech.* **89** 117–31

Carreau P J, De Kee D and Chhabra R 1997 *Capillary Rheometry, Rheology of Polymeric Systems—Principles and Applications* (München: Hanser)

Chen C-S, Chen S-C, Liaw W-L and Chien R-D 2008 Rheological behavior of POM polymer melt flowing through micro-channels *Eur. Polym. J.* **44** 1891–8

Chien R-D, Jong W-R and Chen S-C 2005 Study on rheological behavior of polymer melt flowing through micro-channels considering the wall-slip effect *J. Micromech. Microeng.* **15** 1389–96

Eringen A C and Okada K 1995 A lubrication theory for fluids with microstructure *Int. J. Eng. Sci.* **33** 2297–308

Giboz J, Copponnex T and Mele P 2007 Microinjection molding of thermoplastic polymers: a review *J. Micromech. Microeng.* **17** R96–109

Gleißle W and Windhab E 1985 The 'twin capillary' a simple device to separate shear- and slip-flow of fluids *Exp. Fluids* **3** 177–80

Hatzikiriakos S G and Dealy J M 1992 Wall slip of molten high density polyethilenes: II. Capillary rheometer studies *J. Rheol.* **36** 703–41

Heckele M and Schomburg W K 2004 Review on micro molding of thermoplastic polymers *J. Micromech. Microeng.* **14** R1–14

Kim D S, Lee K C, Kwon T H and Lee S S 2002 Micro-channel filling flow considering surface tension effect *J. Micromech. Microeng.* **12** 236–46

Lee K and Mackley M R 2000 The significance of slip in matching polyethylene processing data with numerical simulation *J. Non-Newton. Fluid Mech.* **94** 159–77

Martin M T, Whiteside B, Coates P D, Allan P S, Greenway G and Hornsby P 2003 Micromoulding: consideration of processing effects on medical materials *ANTEC 2003—61st Annual Technical Conference & Exhibition*

Mitsoulis E, Kazatchkov I and Hatzikiriakos S 2005 The effect of slip in the flow of a branched PP melt: experiments and simulations *Rheol. Acta.* **44** 418–26

Mooney M 1931 Explicit formulas for slip and fluidity *J. Rheol.* **2** 210–23

Piotter V, Hanemann T, Ruprecht R and Haußelt J 1997 Injection molding and related techniques for fabrication of microstructures *Microsyst. Technol.* 129–33

Piotter V, Mueller K, Plewa K, Ruprecht R and Hausselt J 2002 Performance and simulation of thermoplastic micro injection molding *Microsyst. Technol.* **8** 387–90

Rosenbaum E and Hatzikiriakos S 1997 Wall slip in the capillary flow of molten polymers subject to viscous heating *AIChE J.* **43** 598–608

Sha B, Dimov S S, Pham D T and Griffiths C A 2005 Study of factors affecting aspect ratios achievable in micro-injection moulding *Int. Conf. 4M2005.* (Oxford: Elsevier)

Song M C, Liu Z, Wang M J, Yu T M and Zhao D Y 2007 Research on effects of injection process parameters on the moulding process for ultra-thin wall plastic parts *J. Mater. Process. Technol.* **187** 668–71

Su Y C, Shah J and Lin L W 2004 Implementation and analysis of polymeric microstructure replication by micro injection molding *J. Micromech. Microeng.* **14** 415–22

Wagner M H, Schulze V and Göttfert A 1996 Rheotens – Mastercurves and drawability of polymer melts *Polym. Eng. Sci.* **36** 925–35

Yao D and Kim B 2002 Simulation of the filling process in micro-channels for polymeric materials *J. Micromech. Microeng.* **12** 604–10

Zhao J, Mayes R H, Chen G E, Xie H and Chan P S 2003 Effects of process parameters on the micro molding process *Polym. Eng. Sci.* **43** 1542–54